International Journal of Mass Spectrometry 300 (2011) 50–58

Contents lists available at ScienceDirect

International Journal of Mass Spectrometry

journal homepage: www.elsevier.com/locate/ijms

Large ion clusters H_N^+ of Rydberg Matter: Stacks of planar clusters H_7

Leif Holmlid*

Atmospheric Science, Department of Chemistry, University of Gothenburg, SE-412 96 Göteborg, Sweden

ARTICLE INFO

Article history:
Received 2 November 2010
Accepted 10 December 2010
Available online 29 December 2010

PACS:
36.40.−c
61.46.−w
82.30.Nr

Keywords:
Rydberg Matter
Hydrogen
Cluster
Cluster stack
TOF-MS
Coulomb explosion

ABSTRACT

Hydrogen and alkali atoms can form low-density metallic phases, in their most well-ordered form called Rydberg Matter (RM). RM consists mainly of small six-fold symmetric planar clusters in point group D_{6h} as shown by rotational spectroscopy. In their "sleeping top" (dark) state they can form stacks of clusters, as recently observed by ^{39}K nuclear spin-flip transitions. Stacks of clusters H_7 are now directly observed by TOF-MS, using a laser intensity of $<10^{15}$ W cm^{-2}. The TOF-MS resolution is high and the excitation level is found to be $n_B = 1$. The Coulomb explosion process giving the ions observed involves rupture of an H_7 cluster in the stack and probably also addition of a proton to a cluster stack. Further mechanisms are discussed. RM clusters of the stack type can be larger than the previously observed limit for planar RM clusters of $N = 91$. That no $N = 7$ clusters but only larger planar RM clusters were detected in previous rotational spectroscopy studies is now suggested to be due to formation of cluster stacks.

1. Introduction

Clusters of Rydberg Matter are usually small, six-fold symmetric and planar in the point group D_{6h}, as verified by radio-frequency rotational spectroscopy [1,2]. They have been studied by both neutral time-of-flight and TOF-MS using laser-induced Coulomb explosions [3–6] and also by electronic [7], vibrational [8] and rotational [1,2] spectroscopy. RM clusters are easily formed from alkali atoms and hydrogen (protium and deuterium) using heterogeneous catalytic methods [9–11]. Presumably due to retardation effects, the size of RM clusters has been observed to not be larger than $N = 91$, where N is the number of atoms or molecules in the cluster. On the other hand, RM clusters were shown theoretically to be able to form stacks of the clusters, due to the existence of a repulsion barrier between the clusters when they approach sideways [12]. In the stacks, the delocalized electrons at high angular momenta l will give a large magnetic field. This magnetic field is strong at the nuclei, and spin-flips of the nuclear spins in ^{39}K atoms in RM cluster stacks at $l = 6$ were recently observed in the radio-frequency range [13]. In such cluster stacks, the large magnetic momenta of the clusters are directed along the stacks, giving also a considerable magnetic field outside the electron orbits. This effect was proposed to give the unexpectedly large magnetic field observed in intergalactic space by Faraday rotation at radio-frequencies [14].

It is of course very interesting to attempt to detect RM cluster stacks by other methods than spectroscopy, for example by TOF-MS as used here. Since the stacks contain a collective sideway interaction between the neighboring clusters, this type of interaction may be more difficult to break by Coulomb repulsion than the normal point-wise interaction of preformed RM clusters to large RM clouds [6,15]. Thus, high laser intensity is needed, which here is solved by focusing a pulsed laser to intensities of the order of 10^{15} W cm^{-2}. Due to the rather weak bonding in RM clusters, intact stacks or fractions of stacks are probably most easily found for low excitation levels n_B (Bohr model principal quantum number which is numerically equal to l). This is so since the bond distances decrease and bond strengths increase at lower excitation levels. Thus, hydrogen clusters are studied here since they exist preferentially in $n_B = 1$ [16,17].

The easiest way to form RM in the laboratory is to use a commercial alkali doped solid catalyst as the emitter in a vacuum [11]: on heating by a few hundred K, the alkali atoms desorb as Rydberg atoms and RM clusters from the surface. The bonding of alkali atoms in such catalytic materials was recently investigated by EPR studies and DFT cluster model calculations [18]. The authors of Ref. [18] state that the K atom is in an "expanded" state and show that the spin density at the nucleus decreases, which is a typical Rydberg-

* Tel.: +46 31 786 9076.
E-mail address: holmlid@chem.gu.se

1387-3806/$ – see front matter © 2011 Elsevier B.V. All rights reserved.
doi:10.1016/j.ijms.2010.12.008

like effect. They also compare the effect observed to "gas-phase S excited states of the alkali metals" which are approaching the Rydberg form. By admission of hydrogen gas to the emitter material, RM of hydrogen atoms is easily formed [16], in excitation levels n_B = 1–4 depending on the conditions.

A few possible applications of RM should be mentioned. Recently, the possibility of using hydrogen or deuterium in low excitation levels as a fusion fuel in (laser or particle beam driven) inertial confinement fusion (ICF) has received some attention [19,20]. The ultra-dense deuterium material [21,22] is of special interest for this application. Since several years, an effort has been underway to observe RM formed at low temperature by physical methods similar to those used for Bose–Einstein condensation. Progress has been reported in the form of many-body interactions between alkali Rydberg atoms at low temperature [23–25]. Such studies may give a useful form of the future quantum computer as result [26–28]. The formation of RM at alkali promoted catalyst surfaces (as used here) gives a method to measure the activity of the catalysts. For example, suppression of RM and Rydberg species desorption from catalyst surfaces is shown to accompany decreased activity due to poisoning of the catalysts [29]. It was recently suggested that many chemical process applications which require a large energy input like reforming of carbon dioxide to useable fuels will be possible using RM as the catalytic promoter [6]. RM is used successfully in high temperature plasma-based energy conversion devices, like thermionic energy converters [30,31], giving highly improved efficiency of conversion from heat to electric power. RM (in Ref. [30] also named CES (condensed excited states), the term used by Manykin et al. [32]) was there shown to be formed and give special properties for the thermal Cs plasma. In this case, the unique, extremely low work function of RM [33] caused by the large distance between the alkali atoms is used to improve efficiency.

2. Theory

Rydberg Matter was predicted by Manykin et al. around 1980 [32,34,35] as a condensed phase of excited metal atoms, and was used in the literature for the first time to explain experimental results on large field ionizable clusters of Cs in 1991 [36]. The conduction band electrons in RM are excited and delocalized. Thus, the properties of RM are those of a condensed metallic phase, not of separate Rydberg species. The principal quantum number n for separate atoms is replaced by an excitation level n_B (B for Bohr model) in the condensed phase. Theoretical classical calculations with electron correlation [37] show that, even though the RM electrons are delocalized in the RM clusters, it is still possible to describe them as moving in stable circular orbits that are scaled by $n_B{}^2$. Further, it was concluded that bonding may only exist when the electrons have the same excitation level in the RM cluster: dephasing will otherwise take place. Thus each classically stable orbit determines the interionic bond length

$$d = 2.9 n_B{}^2 a_0 \quad (1)$$

where a_0 is the Bohr radius of 52.9 pm. The approximate scale factor 2.9 is determined in quasi-classical stability calculations of RM clusters [37]. It has been determined with high precision by rotational spectroscopy of RM clusters [1] and shown to vary slightly with cluster size N and excitation level n_B [2].

The electric field of the laser beam interacts with RM. As a laser pulse passes through the RM cloud, the electric field due to the laser may excite one or two conduction electrons in the same RM cluster (or two adjacent RM clusters in a stack). Such excited states are more localized than the ground state, which means that the shielding between two ion cores may be temporarily removed by the excitation. The radiative lifetime of such an excited state will be of the order of ns since the transition is allowed. It is also possible that the electrons are removed by the strong laser field. If the shielding is removed at a suitable point like in a bridge between a small cluster and a large cluster, the resulting Coulomb repulsion may break the bridge. If the shielding is removed inside a cluster, more complex processes may take place. If the cluster is small enough, a complete fragmentation of the cluster may result. Coulomb repulsion makes the ions move apart rapidly, within a few ps, which is the Coulomb explosion (CE) process. In this way an RM cluster is released. In a CE in an RM bond with distance d as given in Eq. (1), the potential energy which pushes the two charges apart is

$$W = \frac{e^2}{4\pi\varepsilon_0 d} \quad (2)$$

Thus, a measurement of the kinetic energy released in the explosions W gives the bond distance d and thus also the excitation level n_B. Coulomb explosions in clusters are often highly asymmetric as is well known, giving almost all the KER to the light fragment. This can be understood further from unimolecular reaction theory, since the probability of finding enough energy in one degree of freedom is larger than finding the limited amount of energy distributed correctly in a large number of degrees of freedom. It also requires much less energy on average. The detailed CE process described above will only work for processes where a preformed cluster is released, and possible processes for the breaking of cluster stacks of the type shown in Fig. 1 will be discussed below based on the experimental results. For heavy clusters the kinetic energy in the fragment may be smaller than Eq. (2) predicts. In Table 1, the values of d and W are given for the excitation levels n_B = 1, 3, 4 and 5. The size of the RM cloud is of the order of cm [5].

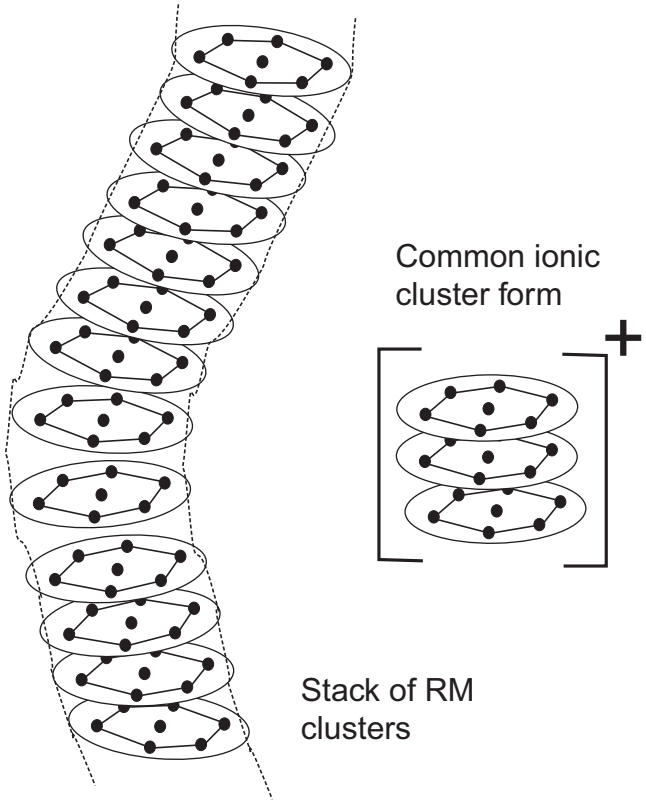

Fig. 1. A stack of H_7 Rydberg Matter clusters, and a common ionic form detected in the TOF-MS experiments.

Table 1
Energy release (KER) in Coulomb explosions and interionic distance in RM as a function of the excitation level n_B, numerically equal to the angular momentum quantum number l of the electrons.

	Excitation level n_B			
	1	3	4	5
Energy release W (eV)	9.38	1.04	0.586	0.375
Interionic distance d (nm)	0.153	1.38	2.46	3.84

3. Experimental

The apparatus has been described in several publications, for example in [16]. The RM emitter can be moved perpendicularly to the laser beam in an UHV chamber with base pressure of 5×10^{-8} mbar. The emitter is a sample of an industrial iron oxide catalyst doped with K (initially at 8 wt%). This catalyst is normally used in the industrial scale production process of styrene from ethyl benzene. The catalyst sample is folded in a Ta foil holder with a flat surface area of 3 mm × 10 mm that is the part exposed to the detector. The emitter is heated by an ac current through the Ta foil to a temperature <500 K. The emitter is connected to a variable voltage, up to 500 V. The distance between the laser focus and the front of the detector is 73 mm, which means electric field strengths up to 70 V cm^{-1}. Hydrogen gas is admitted at a pressure $<1 \times 10^{-5}$ mbar. A Nd:YAG laser gives 5 ns pulses at the wavelength 532 nm. The laser beam is focused at the center of the chamber by a single lens with a focal length of 5 cm. The emitter is moved to a distance of a few mm from the focus. The expanding laser beam passes from the focus and is ended in an Aquadag painted beam dump in cone form at the chamber wall. The maximum pulse energy was 170 mJ. The maximum power density of the beam at the center of the chamber in front of the emitter is calculated from the focusing to be approximately 10^{15} W cm^{-2} at the minimum beam waist of 2 μm. A spherical lens was used for the focusing, and the intensity given is thus probably an upper limit. The detector is a dynode–scintillator–photomultiplier setup that is described in detail elsewhere [16]. In the detector front, a 3 mm × 18 mm (vertical) opening accepts the particle flux. The detector is movable and located at an angle of 90° or 45° from the incoming laser beam in the present experiments. It measures the TOF-MS spectra of ions released from the emitter. In the detector, the ions are accelerated towards a Cu–Be dynode held at −8.0 kV and converted to electrons, which are accelerated towards a plastic scintillator. The photomultiplier observing the scintillator is Electron Tubes 9813B with single electron rise time of 2 ns, using a voltage of 1700 V and a preamplifier. The signal from the photomultiplier is collected by a multi-channel analyzer (EG&G Ortec Turbo-MCS). The TOF of the RM fragments is measured from the time when the laser pulse enters the chamber. The dwell time used here per channel is 5 ns. Each spectrum consists of a sum of the ion signals from 500 laser shots. The flight path is measured from the laser focus in the center of the chamber to the impact in the detector, and it is 113 mm for the ions observed here as also found with calibrations using known ions [6]. See further in the Appendix.

4. Results

Since the ions observed are formed by Coulomb explosions, they generally have excess kinetic energy (KER) from this process. This means that one TOF-MS spectrum is not enough to observe the value of KER and determine the correct ion mass. Thus, the acceleration voltage is varied systematically, from 500 or 400 V down to 50 or 0 V. This gives several different spectra in each experiment from which it is possible to determine both the ion mass and its initial kinetic energy, and also to verify the TOF path length accurately. Since the displayed resolution is higher at large acceleration voltage, the TOF-MS spectrum at the largest acceleration voltage is often the easiest to assign correctly. Such results are collected in Table 2 for the results given in the figures below, for the TOF spectrum with the largest acceleration energy in each case. To simplify the presentation of the results in most of the figures, the time axes of the individual TOF-MS spectra are recalculated to compensate for the different acceleration voltages by multiplication with a factor proportional to the square root of the acceleration voltage (see Appendix). In the E-compensated plots shown, an ion with zero KER will be at a constant TOF in all the spectra, independent of the actual acceleration voltage. This point is also verified in Appendix. A KER different from zero is then observed directly as a shift in peak position to smaller TOF at lower acceleration voltage (in the top of the plots). Also the size of the KER can be easily estimated from the peak shifts, with the limitation being that often also the peak form is changed. A more accurate analysis of the $m/u = 21$ peak in Fig. 2 is given in Table 3. It is shown there that an initial kinetic energy of 9.4 eV reproduces the measured values within the small measurement uncertainty of ±0.3%.

In Fig. 2 the directly measured data are shown in one case. The plots compensated for the acceleration voltage are shown in Fig. 3. There, the ion peaks are interpreted, with data given in Table 2. The two sharpest peaks are interpreted as due to H_{21}^+ and H_{23}^+. The detection of ions at $N = 13$–14, 21, 28 and higher values 56 and 70 which also are multiples of 7 is remarkable. The normal sequence found in numerous experiments both with protium, deuterium and alkali with $N = 19$, 37, 61 and 91 [3,6] is not observed at all. Thus, the cluster ions are not close-packed planar but exhibit some further structure. Recently, extensive experiments on K_N clusters have identified also other series which lead to ejection of planar clusters of lower symmetry. The values of N found are $N = 6$, 9, 10, 13 and 15, but no clear sequences giving such values are observed here.

Another case is shown in Fig. 4 in a compensated type of plot. The occurrence of peaks with $N = 21$, 23 and 28 is very similar to the case in Fig. 3. However, in this case a clear H_{14}^+ peak is observed, thus without the further fragmentation of H_{14} which is observed in Fig. 3. Heavier clusters are observed, well above the $N = 91$ value which is the largest RM (planar) cluster observed previously. No K_N^+ clusters are observed with the high static electric field strength used here, and the ions observed are not due to K from the emitter. The lack of signal due to K is also partly due to the admission of hydrogen to the catalyst. H and K atoms compete for adsorption sites, which means that K cannot be released from the ferrite structure inside the catalyst. At low acceleration voltage in the top of the figure, cluster forms with N close to 61 and 91, thus planar close-packed clusters, are identified. Thus, there is a transition from planar clusters observed at low static electric fields to stacks of clusters at high static fields. The heavy clusters observed at large acceleration voltage are probably of the stack type and $N = 105$ and 119 matches well.

The experiment shown in Fig. 5 is similar to the other experiments at short TOF but differs in the aspect that the admission of hydrogen gas was cut off. Due to the large absorbed amount of H in the catalyst, the experiment may work for hours even without hydrogen admission. On the other hand, the gas phase of ordinary H_2 is removed when gas admission is cut off. The two strong and sharp peaks interpreted as $N = 21$ and 23 in the previous figures are here found to instead be $N = 20$ and 22. It is likely that there is a connection to the decreased availability of hydrogen atoms in this case. At longer TOF, peaks positioned quite accurately at $N = 49$ and 70 are observed, thus further multiples of 7. They are observed for a large range of acceleration voltages and are thus quite stable forms, with a large KER as seen directly from the figure. This means that they are not clusters of K which can only have a KER of 0.59 eV or lower. The ion masses do not match any K clusters either. No K_N^+ RM clus-

Table 2
Measured time-of-flight (TOF) in μs for the three figures shown. The first column under each figure heading gives the ion mass in mass units u. The columns Calc. shows the calculated TOF for 9.4 eV initial kinetic energy.

Number of $N=7$ clusters	Fig. 3 (500 V)		Calc.	Fig. 4 (400 V)		Calc.	Fig. 5 (500 V)		Calc.
2	13–14	1.96	1.95	14	2.22	2.24	12–14	1.90	1.95
	17	2.19	2.23				17	2.19	2.23
3	21	2.48	2.47	21	2.79	2.73	20	2.40	2.41
	23	2.58	2.59	23	2.92	2.86	22	2.50	2.53
4	28	2.81	2.85	28	3.11	3.15	29	2.92	2.91
7							49	3.71	3.77
8	56	4.03	4.03						
10	70	4.43	4.50				70	4.58	4.50
15				105	6.16	6.08			
17				119	6.48	6.46			

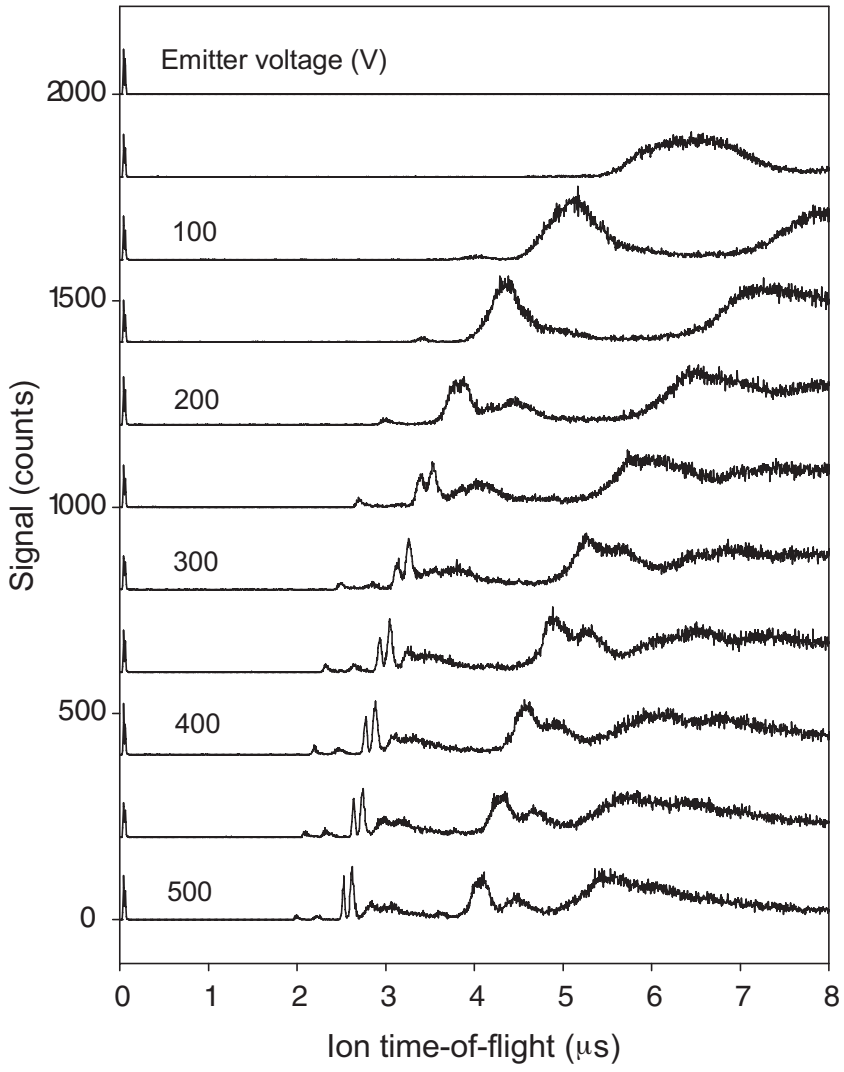

Fig. 2. A TOF-MS experiment with variable acceleration potential, due to the emitter voltage indicated to the left. Note the variation with the voltage. The data are replotted in a different form in Fig. 3.

Table 3
Verification of a kinetic energy of 9.4 eV for ion peak $(H_7)_3^+$ with mass 21 in Figs. 2 and 3. The calculated TOF is for 9.4 eV ion kinetic energy. Below 250 V, this peak is not resolved from mass 23 thus these values are given in parentheses. The last digit corresponds to 10 ns and the accuracy of the TOF measurement is ±10 ns.

	Acceleration voltage (V)								
	500	450	400	350	300	250	200	150	100
Observed TOF (μs)	2.49	2.59	2.73	2.88	3.10	3.35	(3.73)	(4.30)	(5.03)
Calculated TOF (μs)	2.47	2.59	2.73	2.88	3.09	3.34	3.67	4.13	4.86

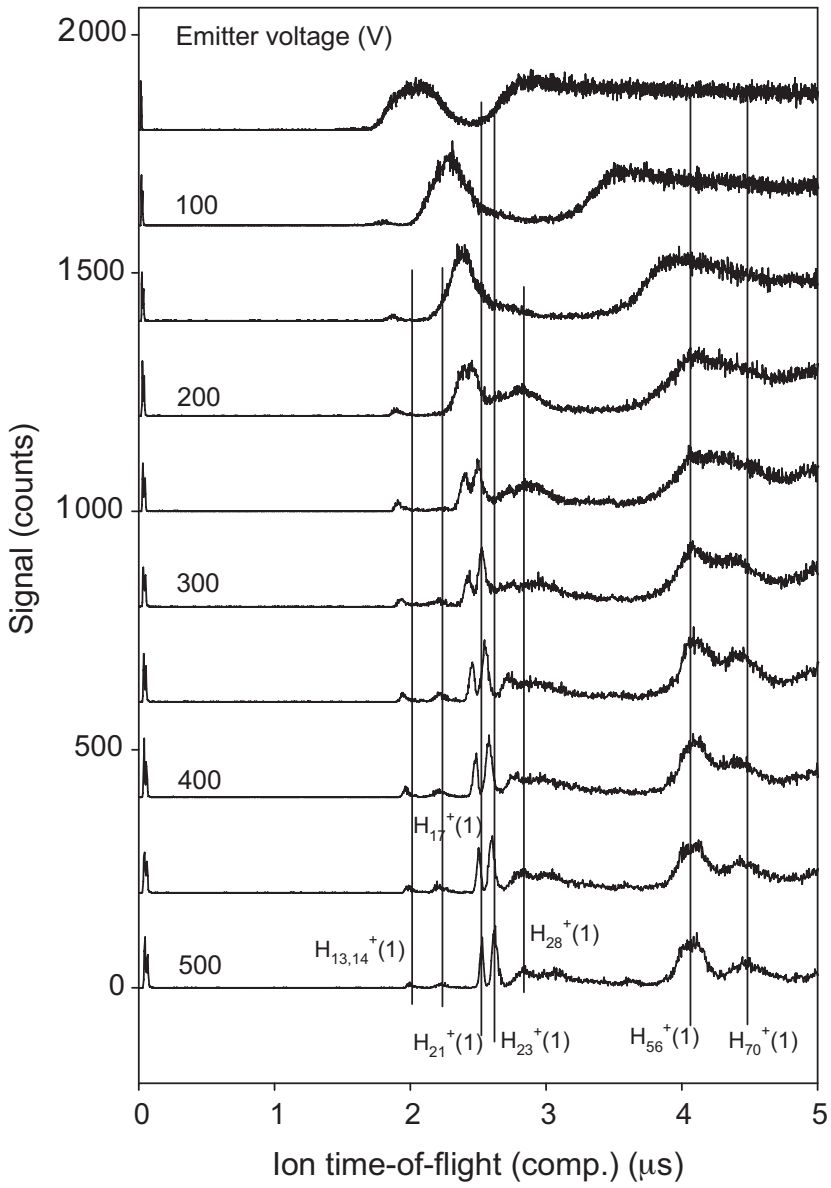

Fig. 3. A plot of TOF-MS data in compensated form, which removes the dependence on the acceleration potential. Note that initial kinetic energy is observed from the peaks moving to the left higher in the plot. The ion peaks are assigned in the figure. Peak values are calculated in Table 2.

ters have ever been observed at the large static field strengths used here, but only at low field strengths (emitter voltages below 25 V) [4,38]. At high field strengths similar to those used here, only ions K^{2+} at mass 19.5 have been observed [6], but not with hydrogen admission which inhibits K desorption.

The excitation level of the part of the cluster stacks that gives the Coulomb explosions can be determined from the measured TOF. The TOF at 500 V acceleration for $N = 21$ is calculated to be 2.47 μs for $n_B = 1$ and 2.65 μs for $n_B = 3$. However, for $N = 22$ the TOF is 2.53 μs for $n_B = 1$. Thus, the excitation level changes the TOF faster than the mass. Due to the experimental situation with high static electric and laser field strengths, it is highly likely that $n_B = 1$ dominates in the RM cloud. See further in Section 5.

5. Discussion

In an ion source with a constant electric field in a system with high KER, the initial ejection of the ions may be in almost any direction, even if the electrons are most likely initially displaced in the direction of the laser electric field. For example, an ion ejected with several eV in the direction opposite to the accelerating field will be decelerated and turned over to follow the electric field direction with a delay relative to those ions initially ejected along the direction of the field. The delay of such turn-around ions has been calculated. No clear peaks are identified as due to such ions. However, some contributions to the low peaks not interpreted in detail here are possible. Due to the slightly non-linear form of the electric potential close to the emitter, a defocusing effect will exist for ions not ejected towards the slit of detector. Thus, turn-around ions are not likely to give any significant contribution to the signal.

The calibration of the mass scale has been done from other studies with for example K^{2+} ions [6] and by using two TOF-MS setups in-line simultaneously [22]. The double TOF-MS method is very reliable, since any effects of field non-linearities become negligible using the long TOF path. A careful analysis of the results found with variable acceleration voltage also shows the calibration to be correct. For example, the first sharp TOF peaks in Fig. 2 are recalculated with variations of mass, KER and TOF distance and found to be well fit by the known TOF distance of 113 mm from other calibrations. The mass was found to be 21 mass units and the

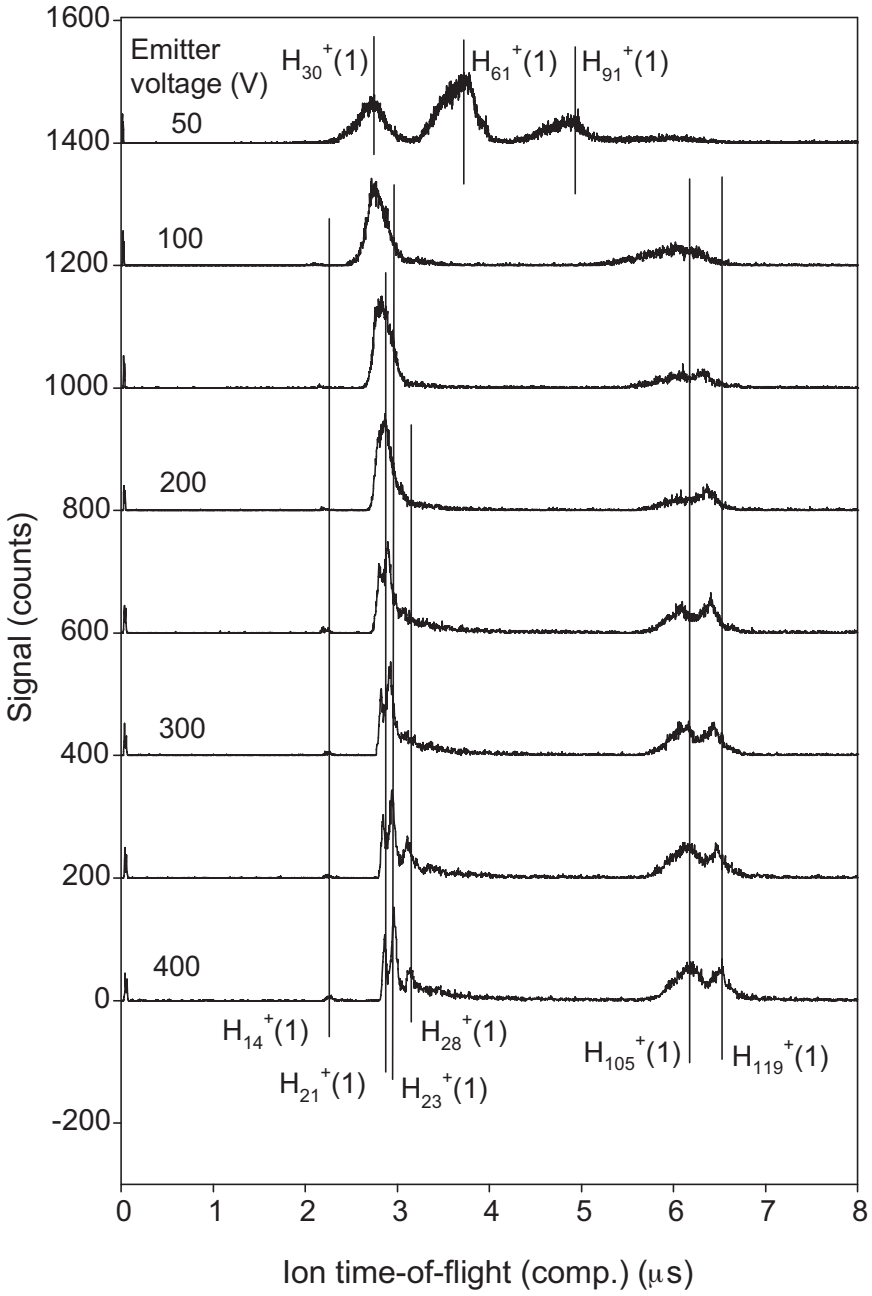

Fig. 4. A compensated plot of TOF-MS results. Note that planar RM clusters are observed at an acceleration (emitter) voltage of 50 V. The ion peaks are interpreted in the figure. Peak values are calculated in Table 2.

KER 9.4 eV, corresponding to excitation level $n_B = 1$. See further in Appendix.

The TOF-MS spectra presented here are not chosen to display the same ion peaks, but rather to show that several different ions can be observed. The different spectra are taken at arbitrary times relative to the start of the laser impact and relative to the periodic movement of the laser to another spot outside the emitter. Thus, the results are snapshots of the fragmentation process, and a complete description of the stepwise destruction of the stacks would require much more data. It has not been possible to follow the development of the various fragments in real time due to the limited signal intensity.

If an ion is ejected from a heavy part of the RM cloud, all the KER will end up in kinetic energy of the ion. In the case of $n_B = 1$ this energy is 9.4 eV. If instead the part from which the ion ejection takes place is of similar mass, approximately half of this energy will end up in each fragment, i.e., 4.7 eV. Intermediate cases may of course also exist. From the figures, it is very clear that almost all ion peaks have a high initial kinetic energy, since the peaks move to shorter TOF at lower acceleration voltages. The results are well fitted by the simplest assumption of the full KER of 9.4 eV given to the ion. An accurate test is given in Table 3, showing a very good agreement for a kinetic energy of 9.4 eV. Thus there is no evidence of any process but an ejection of a relatively small ion cluster from a large heavy part of material. This is reasonable if the RM cloud consists of a large density of long stacks connected together. Due to the strong applied static electric field at high acceleration voltages, RM clusters with large excitation levels and also of planar form are field ionized and removed from the region in front of the emitter. This is seen directly in Fig. 4 where large planar clusters are observed at low field strength but not at high field strengths. Thus, it is concluded that the smallest regular clusters $H_7(1)$ are the clusters most

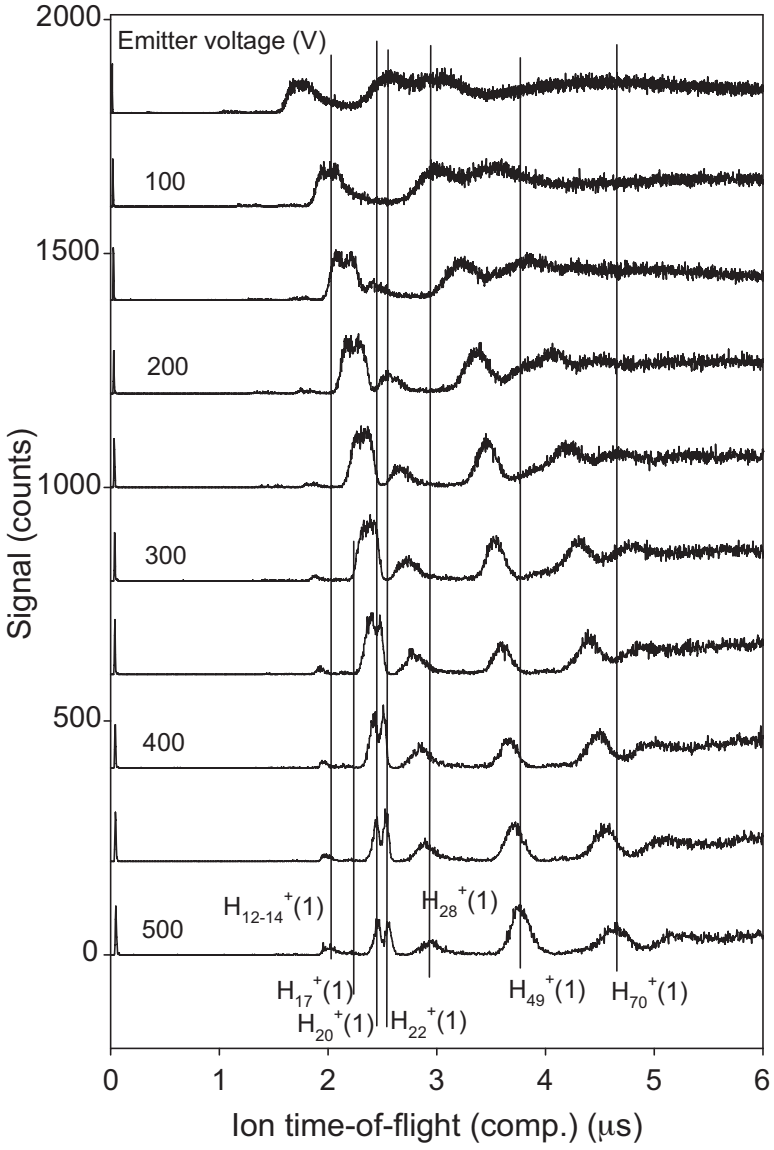

Fig. 5. A compensated plot of the TOF-MS results. No admission of hydrogen gas during this experimental run. The ion peaks are interpreted in the figure. Peak values are calculated in Table 2.

resistant to field ionization since they are small, have strong bonds and probably also since they easily form stacks of clusters.

Small cluster ions of the type $H_N(1)$ have previously been studied at slightly lower electric field strengths and much lower laser intensity [15]. It was found that symmetric forms H_4^+, H_6^+ and H_{12}^+, i.e., tetrahedron, octahedron and (hollow) icosahedron ion clusters were formed due to the closepacked structure of the material H(1). Other small, probably planar clusters like H_7^+ were found but at lower signal intensities. The excitation level $n_B = 1$ was verified from the KER of 9.4 eV. In the present study with much higher laser intensity, such preformed clusters are not evident, but larger clusters from the H(1) "backbone" structure are observed instead.

Some ions observed are not of the simple $N = 7 \times j$ form but rather $N = 7 \times j \pm 1$ or even $N = 7 \times j + 2$. This is most easily observed for the sharp peaks around $N = 21$. In the most common case, $N = 21$ and 23 are found, indicating that the ion cluster stack can add two hydrogen atoms to form $N = 23$. In most experiments, there will exist a large number of both hydrogen atoms and hydrogen molecules at the emitter surface, and the addition of hydrogen atoms (or protons) at the ends of the cluster stack seems likely. It is possible that the charge of the stack is in the form of a proton added to a neutral RM cluster stack, since there is then no added electron to interfere with the RM electrons (which might lead to rapid breakdown of a cluster). This could in fact be one mechanism of ion ejection, by attachment of a proton with 9.4 eV kinetic energy to a free cluster stack. The bond energy of an H atom in H(1) is apparently larger than 9.4 eV, since otherwise clusters with this kinetic energy would not be observed at all. Thus, a proton addition process is likely. In the experiment in Fig. 5, $N = 20$ and 22 are found instead of $N = 21$ and 23. In this experiment, there was no hydrogen gas admission, and the density of hydrogen atoms was lower at the emitter. Thus, the cluster stack has not been able to add more than one proton, and even seems to accidentally have lost a hydrogen atom. Such more complex processes are expected, since the Coulomb explosion ejecting the cluster stack may operate within a cluster. It may be the rupture of one H_7 cluster in the cluster stack that breaks it apart. Thus, it should be possible to observe stacks with incomplete clusters. This is probably the reason why clusters H_{17} are detected among the other more closed stack structures. It may contain an H_7 cluster broken apart. It is interesting to note that the H_{17} peak does not shift strongly towards shorter TOF at lower acceleration potentials: thus, the KER is lower for this odd type of

peak which indicates that it is due to rupture of a cluster inside the stack.

The present study indicates that small clusters H_7 form stacks of clusters much more easily than large clusters like H_{19}. This result agrees with the radio-frequency spectroscopy results on K(RM) clusters [1,2]. In these studies, all planar six-fold symmetric cluster forms with $N = 19$, 37, 61 and 91 were observed clearly and their rotational constants were measured with high precision. However, no rotational spectrum of K_7 was found, despite the detection of such clusters in Coulomb explosion studies [4–6,39]. This is now nicely explained by the formation of stacks of K_7 clusters, since in such stacks the clusters rotate around their main figure axis. This gives no varying dipole moment during their rotational motion and they are thus dark (invisible). However, laser pulses will interact directly with the electrons and lead to Coulomb explosions also in such stacks of clusters, as shown here. Thus, the present study explains the lack of detection of $N = 7$ in the spectroscopic studies.

The clusters in the stacks are bound to each other, and it seems that they are not independent but coupled electronically. This conclusion is based on the long series of spin-flip transitions in ^{39}K nuclei in the field due to inner Rydberg electrons at $n''_B = 5$ and 6 [13]. The long series of spin-flip transitions that are observed in Ref. [13] are only possible if the nuclei are coupled together in the cluster stacks. Thus, the stacks are molecular in character, not only bound by some type of weak forces. This is certainly in agreement with the results presented here, where the ion clusters are bound to each other with bonds that are strong enough to hold even during the Coulomb explosions with KER of 9.4 eV for excitation level $n_B = 1$.

6. Conclusions

It is shown by TOF-MS that clusters H_7 form stacks of Rydberg Matter (RM) clusters, with at least ten clusters in an ion stack. Cluster stacks containing more than the limit of 91 atoms observed previously for planar RM clusters are identified. One common ionic fragment contains three clusters, and the form with two extra atoms added to a three-cluster stack is also common. At the highest static electric field strengths of 70 V cm^{-1} used, the H(RM) structure that survives field ionization is mainly in the form of cluster stacks. The excitation level of this structure is the lowest possible at $n_B = 1$. Formation of cluster stacks is the probable reason why K_7(RM) clusters were not detected by radio-frequency rotational spectroscopy while clusters with 19, 37, 61 and 91 atoms were measured.

Appendix. TOF-MS calibration and E-compensated plots

In the present experiments, an electric field is applied between the catalytic emitter and the front of the detector housing. This means that the cloud of RM outside the emitter front is quite dilute due to constant field ionization of desorbed Rydberg species. Thus, mainly ions are observed from the laser probing of the RM cloud via CE processes, since the formation of neutral RM fragments requires resonance neutralization in the RM cloud. The ions ejected are accelerated towards the detector front where a small part of them enter through the slit opening. This opening has a narrow outer slit and an inner slit approximately 10 mm behind, so that field penetration into the detector housing is small. This TOF-MS setup has been calibrated using many different ions with various kinetic energy (KER) releases, like K^{2+} [6], D^+ [20], small D_N^+ clusters [15,22] and small H_N^+ clusters [15]. By using two TOF-MS detectors simultaneously in direct line-of-sight, the shorter one being the one used here and a longer one with 112 cm flight path, a direct calibration has been done on the same ions with the same KER. This type of calibration has also used more complex ions, like D_N^+ clusters [22]. The response of the TOF-MS to the KER of the ions is the most important point as also described above. Thus it is imperative to perform the calibrations using ions with KER different from zero, as has been done here.

Table 4
The effect of E-compensated ion TOF using mass 21 (H_{21}^+) in calculations with zero KER. Note that the E-compensated TOFs are practically constant for zero KER. This effect is not limited to any special combination of acceleration and field-free regions.

Emitter voltage (V)	Calc. TOF (μs)	E-compensated TOF (μs)
50	8.689	2.748
100	6.159	2.754
150	5.037	2.759
200	4.358	2.756
250	3.897	2.756
300	3.543	2.744
350	3.285	2.748
400	3.076	2.751
450	2.901	2.752
500	2.753	2.753

To visualize the effect of the KER of the ions, so-called E-compensated plots have been used here. This is a reduction of the TOF in the TOF-MS spectra by multiplication with a factor proportional to the square root of the acceleration voltage. It is convenient to use $(U/U_{max})^{1/2}$ as this multiplicative factor, giving a comparison with the spectrum for the highest emitter voltage U_{max}. This reduction gives a constant value of the TOF for peaks with zero KER. This is shown in Table 4, using the calculational procedure employed to interpret the TOF-MS spectra here. This effect is not limited by any special relation between the acceleration and field-free distances in the TOF-MS spectrometer, but is a general scaling feature of the electric field.

References

[1] L. Holmlid, Precision bond lengths for Rydberg Matter clusters K_{19} in excitation levels $n = 4$, 5 and 6 from rotational radio-frequency emission spectra, Mol. Phys. 105 (2007) 933.
[2] L. Holmlid, Rotational spectra of large Rydberg Matter clusters K_{37}, K_{61} and K_{91} give trends in K–K bond distances relative to electron orbit radius, J. Mol. Struct. 885 (2008) 122.
[3] J. Wang, L. Holmlid, Rydberg Matter clusters of hydrogen $(H_2)_N^*$ with well defined kinetic energy release observed by neutral time-of-flight, Chem. Phys. 27 (2002) 201.
[4] L. Holmlid, The alkali metal atmospheres on the Moon and Mercury: explaining the stable exospheres by heavy Rydberg Matter clusters, Planet. Space Sci. 54 (2006) 101.
[5] H. Åkesson, S. Badiei, L. Holmlid, Angular variation of time-of-flight of neutral clusters released from Rydberg Matter: primary and secondary Coulomb explosion processes, Chem. Phys. 321 (2006) 215.
[6] A. Kotarba, L. Holmlid, Energy-pooling transitions to doubly excited K atoms at a promoted iron-oxide catalyst surface: more than 30 eV available for reaction, Phys. Chem. Chem. Phys. 11 (2009) 4351.
[7] L. Holmlid, Stimulated emission spectroscopy of Rydberg Matter: observation of Rydberg orbits in the core ions, Appl. Phys. B 87 (2007) 273.
[8] L. Holmlid, Vibrational transitions in Rydberg Matter clusters from stimulated Raman and Rabi-flopping phase-delay in the infrared, J. Raman Spectr. 39 (2008) 1364.
[9] A. Kotarba, A. Baranski, S. Hodorowicz, J. Sokolowski, A. Szytula, L. Holmlid, Stability and excitation of potassium promoter in iron catalysts – the role of $KFeO_2$ and $KAlO_2$ phases, Catal. Lett. 67 (2000) 129.
[10] A. Kotarba, G. Adamski, Z. Sojka, S. Witkowski, G. Djega-Mariadassou, Potassium at catalytic surfaces – stability, electronic promotion and excitation, in: International Congress on Catalysis, 2000, Pt A, Stud. Surf. Sci. Catal. 130A (2000) 485.
[11] L. Holmlid, Conditions for forming Rydberg Matter: condensation of Rydberg states in the gas phase versus at surfaces, J. Phys.: Condens. Matter 14 (2002) 13469.
[12] S. Badiei, L. Holmlid, Rydberg Matter in space – low density condensed dark matter, Mon. Not. R. Astron. Soc. 333 (2002) 360.
[13] L. Holmlid, Nuclear spin transitions in the kHz range in Rydberg Matter clusters give precise values of the internal magnetic field from orbiting Rydberg electrons, Chem. Phys. 358 (2009) 61.
[14] S. Badiei, L. Holmlid, Magnetic field in the intracluster medium: Rydberg Matter with almost free electrons, Mon. Not. R. Astron. Soc. 335 (2002) L94.

[15] L. Holmlid, Clusters H_N^+ ($N = 4, 6, 12$) from condensed atomic hydrogen and deuterium indicating close-packed structures in the desorbed phase at an active catalyst surface, Surf. Sci. 602 (2008) 3381.
[16] S. Badiei, L. Holmlid, Experimental studies of fast fragments of H Rydberg Matter, J. Phys. B: At. Mol. Opt. Phys. 39 (2006) 4191.
[17] S. Badiei, L. Holmlid, Laser initiated detonation in Rydberg Matter with a fast propagating shock wave, releasing protons with keV kinetic energy, Phys. Lett. A 344 (2005) 265.
[18] M. Chiesa, E. Giamello, C. Di Valentin, G. Pacchioni, Z. Sojka, S. Van Doorslaer, Nature of the chemical bond between metal atoms and oxide surfaces: new evidences from spin density studies of K atoms on alkaline earth oxides, J. Am. Chem. Soc. 127 (2005) 16935.
[19] S. Badiei, L. Holmlid, Condensed atomic hydrogen as a possible target in inertial confinement fusion (ICF), J. Fusion Energy 27 (2008) 296.
[20] P.U. Andersson, L. Holmlid, Ultra-dense deuterium: a possible nuclear fuel for inertial confinement fusion (ICF), Phys. Lett. A 373 (2009) 3067.
[21] S. Badiei, P.U. Andersson, L. Holmlid, Fusion reactions in high-density hydrogen: a fast route to small-scale fusion? Int. J. Hydr. Energy 34 (2009) 487.
[22] S. Badiei, P.U. Andersson, L. Holmlid, High-energy Coulomb explosions in ultra-dense deuterium: time-of-flight mass spectrometry with variable energy and flight length, Int. J. Mass Spectrom. 282 (2009) 70.
[23] I. Mourachko, W. Li, T.F. Gallagher, Controlled many-body interactions in a frozen Rydberg gas, Phys. Rev. A 70 (2004) 031401.
[24] W.R. Anderson, M.P. Robinson, J.D.D. Martin, T.F. Gallagher, Dephasing of resonant energy transfer in a cold Rydberg gas, Phys. Rev. A 65 (2002) 063404.
[25] J.-H. Choi, B. Knuffmann, T. Cubel Liebisch, A. Reinhard, G. Raithel, Cold Rydberg atoms, Adv. At. Mol. Opt. Phys. 54 (2006) 132.
[26] R. Côté, Quantum computing with Rydberg atoms, Proc. SPIE 6014 (2005) 601415.
[27] E. Brion, K. Mølmer, M. Saffman, Quantum computing with collective ensembles of multilevel systems, Phys. Rev. Lett. 99 (2007) 260501.
[28] M. Weidemüller, C. Zimmermann (Eds.), Cold Atoms and Molecules, Concepts, Experiments and Applications to Fundamental Physics, Wiley-VCH, 2009.
[29] A. Kotarba, J. Dmytrzyk, U. Narkiewicz, A. Baranski, Sulfur poisoning of iron ammonia catalyst probed by potassium desorption, React. Kinet. Catal. Lett. 74 (2001) 143.
[30] V.I. Yarygin, V.N. Sideĺnikov, I.I. Kasikov, V.S. Mironov, S.M. Tulin, Experimental study on the possibility of formation of a condensate of excited states in a substance (Rydberg Matter), JETP Lett. 77 (2003) 280.
[31] R. Svensson, L. Holmlid, Electronic Raman processes in Rydberg Matter of Cs: circular Rydberg states in Cs and Cs^+, Phys. Rev. Lett. 83 (1999) 1739.
[32] É.A. Manykin, M.I. Ozhovan, P.P. Poluéktov, Theory of the condensed state in a system of excited atoms, Sov. Phys. JETP 57 (1983) 256.
[33] M. Svanberg, L. Holmlid, Work function of Rydberg Matter surfaces from jellium calculations, Surf. Sci. 315 (1994) L1003.
[34] É.A. Manykin, M.I. Ozhovan, P.P. Poluéktov, Transition of an excited gas to a metallic state, Sov. Phys. Tech. Lett. 6 (1980) 95.
[35] É.A. Manykin, M.I. Ozhovan, P.P. Poluéktov, Condensed states of excited cesium atoms, Sov. Phys. JETP 75 (1992) 440.
[36] C. Åman, J.B.C. Pettersson, L. Holmlid, Field ionizable cesium metal clusters from a foil diffusion source, Chem. Phys. 147 (1990) 189.
[37] L. Holmlid, Classical energy calculations with electron correlation of condensed excited states – Rydberg Matter, Chem. Phys. 237 (1998) 11.
[38] J. Wang, L. Holmlid, Polarization effects in laser photofragmentation of Rydberg Matter clusters K_N^* in a weak electric field, Chem. Phys. Lett. 325 (2000) 264.
[39] S. Badiei, L. Holmlid, Neutral Rydberg Matter clusters from K: extreme cooling of translational degrees of freedom observed by neutral time-of-flight, Chem. Phys. 282 (2002) 137.